Journal of Inorganic Biochemistry 199 (2019) 110793

Contents lists available at ScienceDirect

Journal of Inorganic Biochemistry

journal homepage: www.elsevier.com/locate/jinorgbio

Binding and photodynamic action of the cationic zinc phthalocyanines with different types of DNA toward understanding of their cancer therapy activity

Ewan K.S. McRae, Dustin E. Nevonen, Sean A. McKenna*, Victor N. Nemykin*

Department of Chemistry, University of Manitoba, 144 Dysart Rd, R3T 2N2 Winnipeg, MB, Canada

ARTICLE INFO

Keywords:
Photodynamic therapy
DNA binding
Confocal microscopy
Phthalocyanine
Singlet oxygen generation

ABSTRACT

Two cationic zinc phthalocyanines have been tested for their interactions with several DNA secondary structures. Despite different aggregation properties, both phthalocyanines bind to DNA in monomeric forms. The strong photodynamic activity of phthalocyanines was demonstrated by *in vitro* experiments and correlate well with high singlet oxygen yields determined experimentally with 1,3-diphenylisobenzofurane. Both phthalocyanines accumulate in the cell cytoplasm prior to radiation; however, only the octacationic photosensitizer was observed in the cell nuclei after irradiation.

1. Introduction

Transition metal phthalocyanines (Pcs) are well known functional dyes used as colorants in industry [1–6], active components in information recording devices [7–11], and catalysts [12–16]. It is known that the axially or core-substituted closed-shell Pcs, especially aluminum, silicon, and zinc derivatives, are suitable for applications in photodynamic therapy (PDT) of cancer [17–29]. Indeed, one of the sulfonated aluminum phthalocyanines (AlPcs, also known as Photosense [30,31]) is currently in clinical use in Russia. The key advantages of closed-shell transition metal phthalocyanines for PDT applications lie in their easily tunable optical properties and triplet state formation, which in turn are responsible for effective singlet oxygen production needed for photodynamic action. Recently, studies have been performed on the effectiveness of the polycationic zinc phthalocyanines (ZnPcs) for antimicrobial [32] and anticancer PDT applications [33]; however, unlike in well studied sulfonated AlPc derivatives, very little is known about the binding and photodynamic action of such Pcs with different DNA secondary structures [34–36]. Thus, in this paper we discuss the binding and photodynamic activities of two cationic ZnPcs (**Pc1** and **Pc2**, Chart 1) for single-stranded (SS-DNA), double-stranded (DS-DNA), and G-quadruplex DNA (G4-DNA).

2. Materials and methods

2.1. Materials

The MCF-7 cell line (gift from Dr. Spencer Gibson) was maintained in a humidified incubator at 37 °C with 5% CO_2, grown in Dulbecco's Modified Eagle's Medium (DMEM) (Invitrogen, Burlingon, ON, Canada) supplemented with 10% fetal calf serum (FCS) (Invitrogen). DNA substrates were purchased desalted and lyophilized from Integrated DNA technologies (IDT). The following sequences of DNA were used: SS-DNA (5′AGCGTTAGCGTTAGCGTTAGCG3′), DS-DNA was formed by the addition of (5′CGCTAACGCTAACGCTAACGCT3′) to the SS-DNA, G4-DNA (5′AGGGTTAGGGTTAGGGTTAGGG3′). Phthalocyanine samples **Pc1** and **Pc2** were received from Professor E. A. Lukyanets. 1,3-Diphenylisobenzofurane was purchased from Sigma and used as received.

2.2. UV–vis and MCD spectroscopy

UV–vis spectra were collected on a Jasco V-770 spectrophotometer and magnetic circular dichroism (MCD) spectra were measured with a Jasco J-1500 CD spectrometer using a Jasco MCD-581 electromagnet which was operated at 1.0 T. The absorption spectra for the DNA titrations were collected with a Varian Cary 50 spectrophotometer and the fluorescence data were measured on a Varian Eclipse spectrofluorometer.

2.3. DNA binding titrations and singlet oxygen yields

All absorbance titrations were run in an aqueous 50 mM 2-(*N*-morpholino)ethanesulfonic acid (MES) buffer (pH = 7.0) and 100 mM KCl mixed solution. **Pc1** and **Pc2** were diluted until a nominal absorbance of 2 A.U. at the Soret/Q-band was achieved in the optical spectrum. A 100 μM solution of DNA was prepared by heating the dissolved

* Corresponding authors.
E-mail addresses: Sean.McKenna@umanitoba.ca (S.A. McKenna), Victor.Nemykin@umanitoba.ca (V.N. Nemykin).

https://doi.org/10.1016/j.jinorgbio.2019.110793
Received 16 April 2019; Received in revised form 22 July 2019; Accepted 23 July 2019
Available online 24 July 2019
0162-0134/

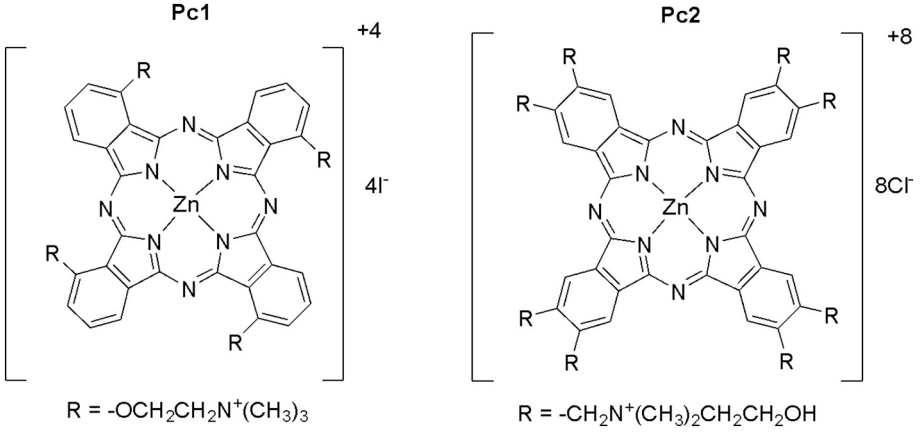

Chart 1.

DNA to 95 °C for 5 min before a slow cooling to room temperature (5 °C/min). Absorption and fluorescence spectra were collected after each 1 μL addition of DNA solution until saturation was achieved. Singlet oxygen yields were determined using 1,3-diphenylisofurane as a singlet oxygen scavenger following standard procedure [37]. The custom-made apparatus used was a 100 W white-light bulb in a 60 W lamp which was equipped with a 630–760 nm band pass filter. The intensity was calculated to be 1326 W/m^2. A 1 cm cuvette was used for all experiments. In all experiments, concentration of **Pc1** and **Pc2** in a buffer solution was held between 10^{-5} and 10^{-6} M.

2.4. Cell culture and reagents

MCF-7 cells were seeded at 50,000 cells per well in 24-well cell culture plates (Thermo-Fisher Scientific). **Pc1** and **Pc2** compounds were dissolved in water and sterilized using a 0.22 μM cellulose syringe filter prior to cell treatments. After 24 h, **Pc1** or **Pc2** or water was added to the cell culture media to a final concentration of 5 μM and incubated at 37 °C 5% CO_2 for a further 24 h. The cells were then rinsed with PBS and the media replaced with fresh DMEM + FCS. For the experiments with fixed cells, the samples were irradiated (or not) for 5 min with a FluorChem Q imager (Protein Simple) using the CY5 excitation filter (620–720 nm band pass). Cells were returned to the incubator for 4 h before imaging. Immunofluoresence experiments were performed as described previously [38] using AlexaFluor 488 conjugated anti-H2A.X (P139S) antibody (Thermo-Fisher Scientific, CR55T33), Prolong Diamond mounting media containing DAPI (4′,6-diamidino-2-phenylindole, Thermo-Fisher Scientific) and imaged at 40× using an EVOS FL Auto imaging system (Thermo-Fisher Scientific). For live cell imaging, samples were irradiated for only 1 min before the cell culture media was changed to Live Cell Imaging Solution (Thermo-Fisher Scientific) and the cells were imaged on the EVOS FL Auto imaging system. Individual wells were used for each time point to minimize the effect of additional reactive oxygen species (ROS) produced by imaging the phthalocyanine compounds (using the CY5 filter with band pass between 620 and 700 nm) that would affect the progression of cell death in further time points. The LD50 for **Pc1** and **Pc2** were not calculated; the non-irradiated cells did not suffer from the treatment and the signal from the H2AX antibody is very close to background with no distinct foci observed.

2.5. DFT calculations

Density Functional Theory (DFT) and Time-Dependent DFT (TDDFT) calculations were conducted using Gaussian 09 software [39]. Hybrid TPSSh exchange-correlation functional [40] was used in all cases. A standard 6-311G(d) basis set was used for all atoms [41]. The first 80 excited states were considered in TDDFT calculations. Molecular orbital compositions were determined using QMForge software [42] and the frontier orbitals were visualized using GaussView program.

3. Results and discussion

3.1. UV–vis and MCD spectra

It is well-known that the formation of phthalocyanine H-aggregates results in a blue-shift of the low-energy Q-band, reduces phthalocyanines' fluorescence quantum yield and diminishes PDT activity [43–47]. Thus, it was important to evaluate aggregation behavior of the **Pc1** and **Pc2** in water as physiological solvent. The UV–vis and MCD spectra of tetracationic and octacationic zinc phthalocyanines **Pc1** and **Pc2** in water are shown in Fig. 1.

In both cases, the Q-band can be identified as a strong MCD *A*-term centered at 695 nm (**Pc1**) or 679 nm (**Pc2**). It is clear from the UV–vis and MCD spectra that in water the degree of aggregation of tetracationic **Pc1** is significantly higher than that in **Pc2**. In the case of **Pc2**, the Q-band shoulder centered at 613 nm can be clearly seen in its UV–vis spectrum and is associated with the positive MCD signal at 617 nm. In contrast, a broad band at ~650 nm was observed in the case of **Pc1** in water, and is associated with a very strong positive signal in the MCD spectrum centered at 634 nm. From the MCD spectra, the intensity ratio of signals between the positive portion of the *A*-term at 667 nm and shoulder at 617 nm is clearly much larger for **Pc2** compared to the same ratio between positive signals at 686 (*A*-term) and 634 (shoulder) nm for **Pc1**. The appearance of the broad, positive MCD signal at 634 nm in the case of **Pc1** is indicative of the formation of H-aggregates in solution for this compound [48–52]. The formation of aggregates in **Pc1** was further confirmed by its UV–vis spectra taken in methanol and DMSO solutions, where the monomeric form of **Pc1** dominates the spectrum (Fig. 2).

The formation of H-aggregates in the case of **Pc1** can be easily explained by its lower positive charge compared to **Pc2** where its octacationic nature precludes π-π interactions between two phthalocyanine cores due to strong electrostatic repulsion. As expected, the introduction of four electron donating groups to α-positions on the core of **Pc1** resulted in a significant red-shift of the Q-band compared to **Pc2** (705 nm in DMSO for **Pc1** monomer *vs.* 682 nm in DMSO for **Pc2** monomer).

3.2. DFT and TDDFT calculations

In order to correlate the red-shifts in **Pc1** *versus* **Pc2** with their electronic structures, Density Functional Theory (DFT) calculations

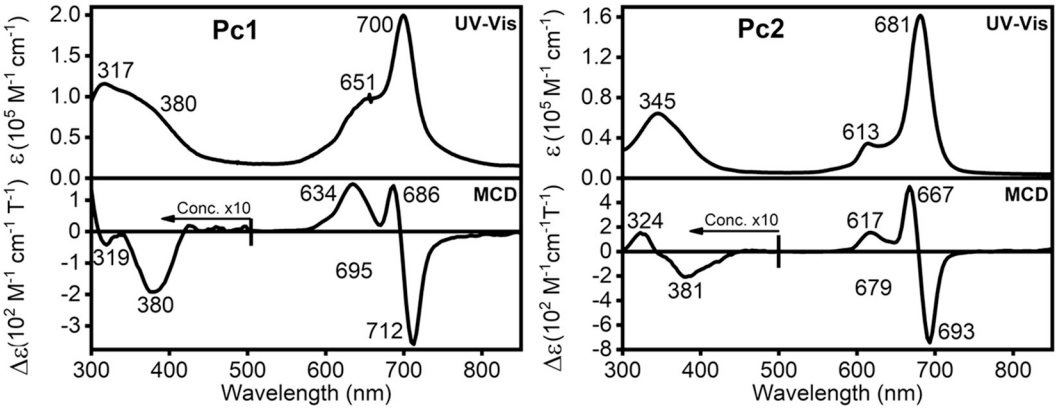

Fig. 1. UV–vis and MCD spectra of **Pc1** and **Pc2** in water.

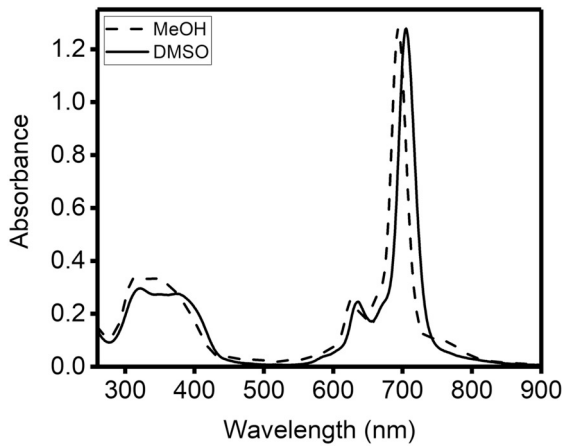

Fig. 2. UV–vis spectra of **Pc1** in methanol and DMSO.

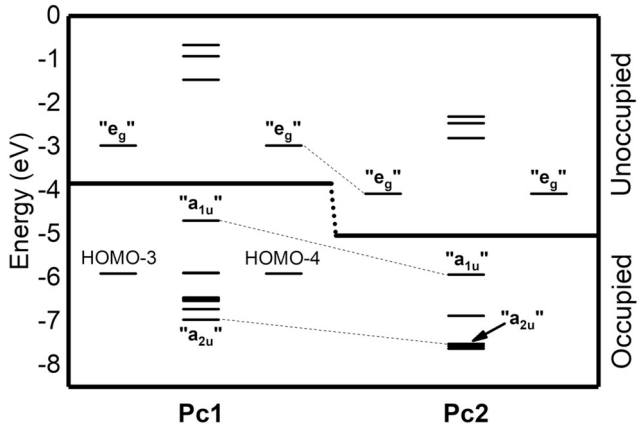

Fig. 3. DFT-predicted energy level diagram for **Pc1** and **Pc2**.

were conducted on both compounds. The DFT-predicted energy diagram is shown in Fig. 3 and frontier orbitals are pictured in Fig. 4.

In both cases, the DFT-predicted highest occupied molecular orbital (HOMO) orbital resembles the classic Gouterman's "a_{1u}" and the lowest unoccupied molecular orbital (LUMO) and LUMO + 1 orbitals resemble Gouterman's "e_g" pair of orbitals [53,54]. TDDFT-predicted UV–vis spectra of **Pc1** and **Pc2** are compared to the experimental data in Fig. 5.

In good agreement with the experimental data, the TDDFT-predicted energy of the Q-band in **Pc1** (717 nm) is red-shifted compared to that predicted for **Pc2** (661 nm). In addition, a set of intra-ligand charge-transfer transitions from the electron-donating alkoxy groups to LUMO and LUMO + 1 have been predicted by TDDFT for **Pc1** at 457 nm, which is in good agreement with experimental data on **Pc1** and the similar phthalocyanines with electron-donating groups located at the α-positions of phthalocyanine core [55,56].

3.3. Singlet oxygen generation

In order to estimate the potential photodynamic activity of **Pc1** and **Pc2**, singlet oxygen formation yields for these two photosensitizers in DMSO were determined using 1,3-diphenylisobenzofuran (DPBF) as a singlet oxygen scavenger (Fig. 6) [37].

Upon irradiation of **Pc1** and **Pc2** in DMSO/DPBF solutions at Q-band wavelengths, rapid degradation of the singlet oxygen scavenger was observed while no decrease of Q-band intensity was detected. The singlet oxygen generation abilities of **Pc1** and **Pc2** are quite high and virtually equivalent to that observed in unsubstituted ZnPc in DMSO, likely indicative of the minor influence of the peripheral substituents on the formation and lifetime of triplet states in these photosensitizers.

3.4. DNA-binding studies

The interactions between **Pc1** and **Pc2** and DNA have been investigated for SS-DNNA, DS-DNA, and G4-DNA structures, both by UV–vis and fluorescence spectroscopy (Figs. 7 and 8).

Based on these experiments, the binding features of **Pc1** and **Pc2** to all three tested DNA structures were similar. In the case of octacationic, less aggregative **Pc2**, the DNA binding follows the general trend observed for the other phthalocyanine photosensitizers used in PDT of cancer [57–63]. For all three DNA structures, an approximate 10% decrease in intensity and 7 nm red-shift of the Q-band were observed in the corresponding **Pc2** UV–vis spectra. The observed red-shift does not correspond to the monomerization process as solutions of **Pc1** in DMSO and MeOH have a higher-energy Q-band. Such change can only be associated either with DNA-phthalocyanine interaction or J-aggregation. The changes in the Q-band intensity and energy were associated with an initial strong decrease of the fluorescence band observed at 693 nm. During saturation titration experiments an increase in fluorescence intensity at 698 nm was consistently observed (Fig. 8). Again, such behavior is indicative of the strong interaction between **Pc2** photosensitizer and DNA molecules.

The UV–vis and fluorescence DNA titrations data for **Pc1** are quite different as **Pc1** has a higher tendency to form H-aggregates both in water and buffer solutions. Indeed, during the DNA titration experiment, we observed increasing intensity and red-shifting of the Q-band for all three DNA structures tested. This increase in intensity was accompanied by a decrease of the absorption intensity of the H-aggregate of this compound. Thus, we speculate that during DNA binding with **Pc1**, this photosensitizer's H-aggregates convert into the monomeric form of the Pc which binds to DNA. As the monomeric form of the **Pc1**

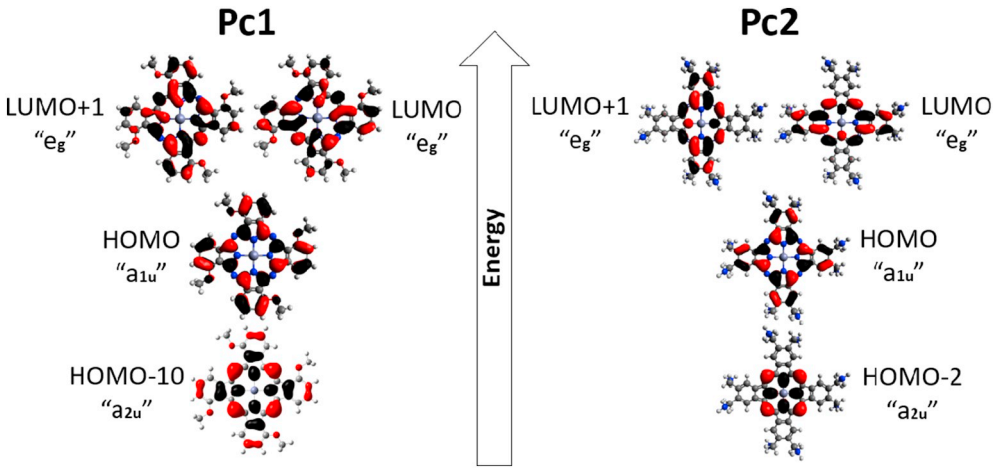

Fig. 4. Frontier molecular orbitals of **Pc1** and **Pc2**.

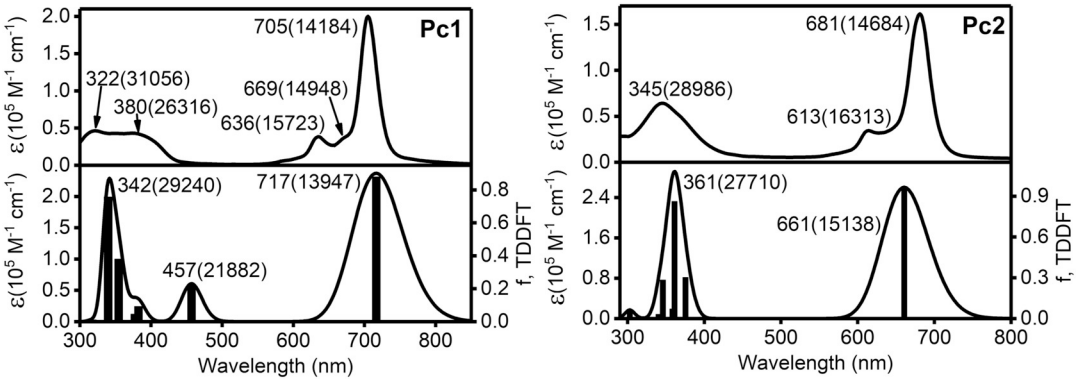

Fig. 5. TDDFT-predicted UV–vis spectra of **Pc1** and **Pc2**. The band units are represented by nm (cm^{-1}).

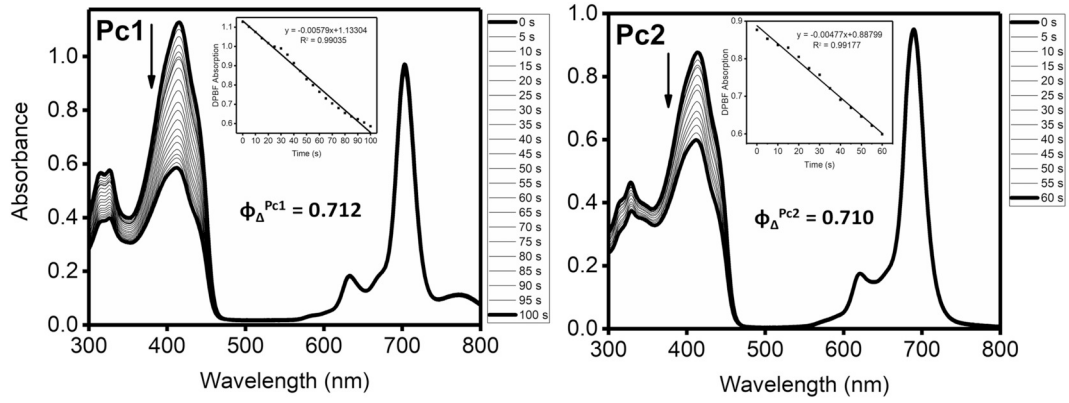

Fig. 6. Singlet oxygen production UV–vis spectra for **Pc1** and **Pc2** in DMSO using DPBF.

has higher DNA-binding affinity (because of the less demanding steric restrictions), and since H-aggregates of Pcs are non-fluorescent in nature [64,65], it was not surprising that an initial decrease in fluorescence intensity was observed (Fig. 7) during titration experiments. However, once non-fluorescent H-aggregates monomerized and interact with DNA, the overall fluorescence of the DNA-**Pc1** assemblies increases as expected (Fig. 7). Overall, these DNA titration experiments suggest strong interactions between both **Pc1** and **Pc2** photosensitizers and all three DNA structures investigated, consistent with non-specific interactions with the phosphodiester backbone. Therefore, there is promise in a broad spectrum of pharmacological activity of **Pc1** and **Pc2** photosensitizers with a variety of DNA structures beyond those tested.

3.5. Photosensitizer/cell interaction study

To evaluate the potential of **Pc2** as a photosensitizer for photodynamic therapy as compared to **Pc1**, the changes in cell morphology, nucleolar compaction, and DNA damage (*via* histone H2AX P139S phosphorylation) in MCF-7 cells that were treated with **Pc1** or **Pc2** both pre- and post-irradiation were compared.

As a reference and control, the top two rows of Fig. 9 show healthy, adherent cells with normal nuclei and only a background signal from the DNA damage marker. As expected, no change is observed if these cells are not irradiated at the appropriate wavelength that excites the dyes. In contrast, cells treated with **Pc1** (Fig. 9) and irradiated show cellular rounding, nuclear compaction and detachment from the

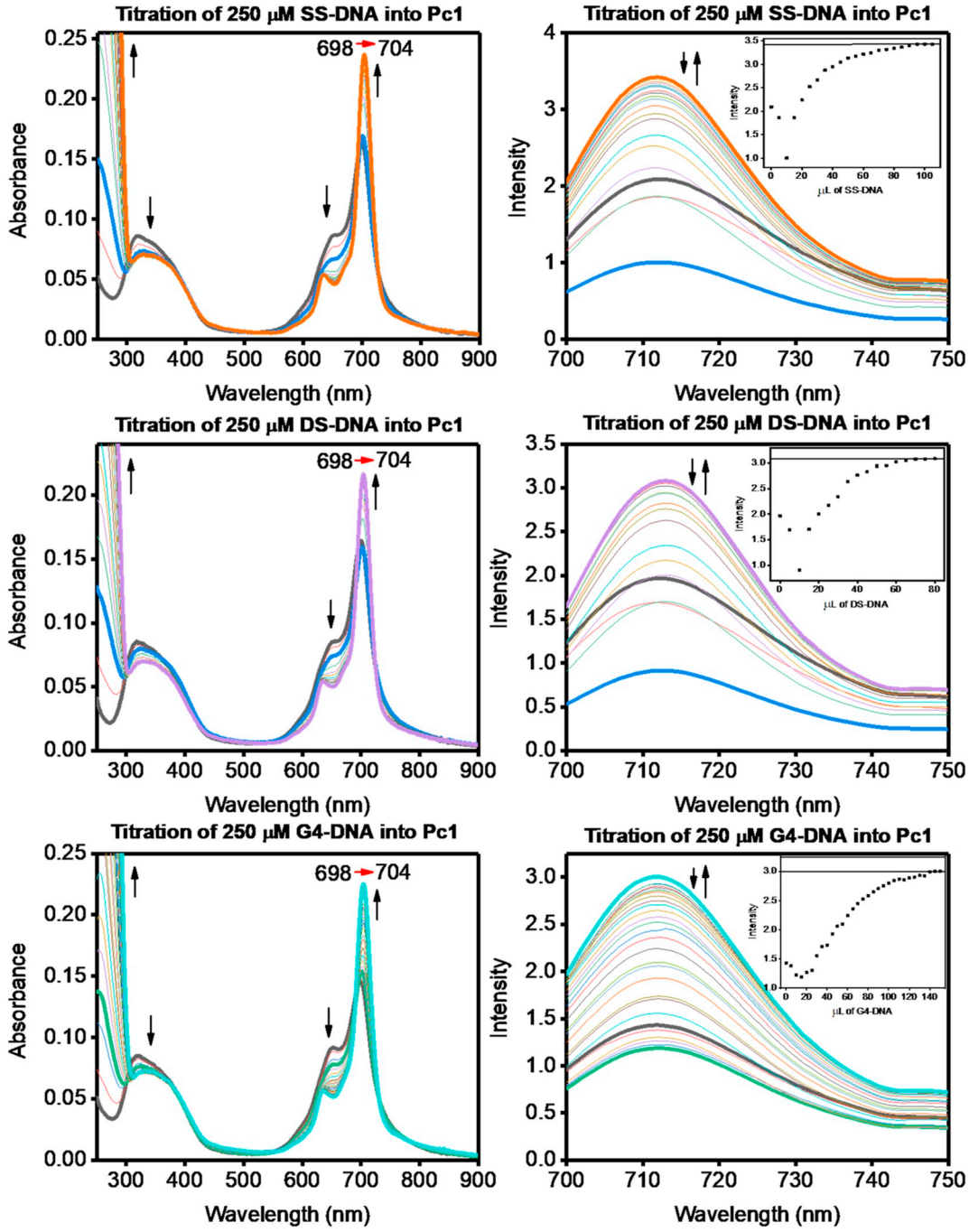

Fig. 7. UV–vis and fluorescence spectra of the DNA titrations involving **Pc1**.

extracellular matrix, consistent with apoptotic cells [66], and DNA damage, a hallmark of PDT [67,68]. Cells that were not irradiated appear healthy but do have a markedly higher background signal from the DNA damage marker than the untreated cells. Direct detection of **Pc1** using the CY5 light filters in the microscope proved troublesome; while some of the dye can be observed by our microscope in the non-irradiated sample, fluorescence is not observed post-irradiation. When **Pc1** was observed pre-irradiation, it appears to be diffuse and in the cytoplasm with some cells having compact granules containing **Pc1** present in their nuclei. The lower photostability of the **Pc1** compared to **Pc2** is not surprising as its DFT-predicted HOMO energy is significantly higher than the HOMO energy in **Pc2**, which makes **Pc1** more prone to oxidative degradation and is in agreement with earlier observations on phthalocyanines bearing electron-donating groups at the α-positions of the macrocyclic core [55,56].

Pc2 treated cells showed a similar response to irradiation as **Pc1** treated cells: detachment, rounding, nuclear compaction, and DNA damage markers were observed (Fig. 9). Unlike **Pc1**, **Pc2** could be observed both pre- and post-irradiation. Like **Pc1**, **Pc2** is mostly diffuse and cytoplasmic before irradiation. Post-irradiation, fluorescence from **Pc2** is localized to the cell nuclei. Of note, is that the background-level signal from the DNA damage marker is significantly less in the non-irradiated **Pc2** treated cells compared to the non-irradiated **Pc1** treated cells. Since mutagenesis of healthy cells that may take up a PDT photosensitizing agent is a concern, the reduced background DNA damage signal from **Pc2** in the non-irradiated cells may indicate it to be of less risk to healthy cells.

Next, we followed the timeline of cell death after irradiating the **Pc1**

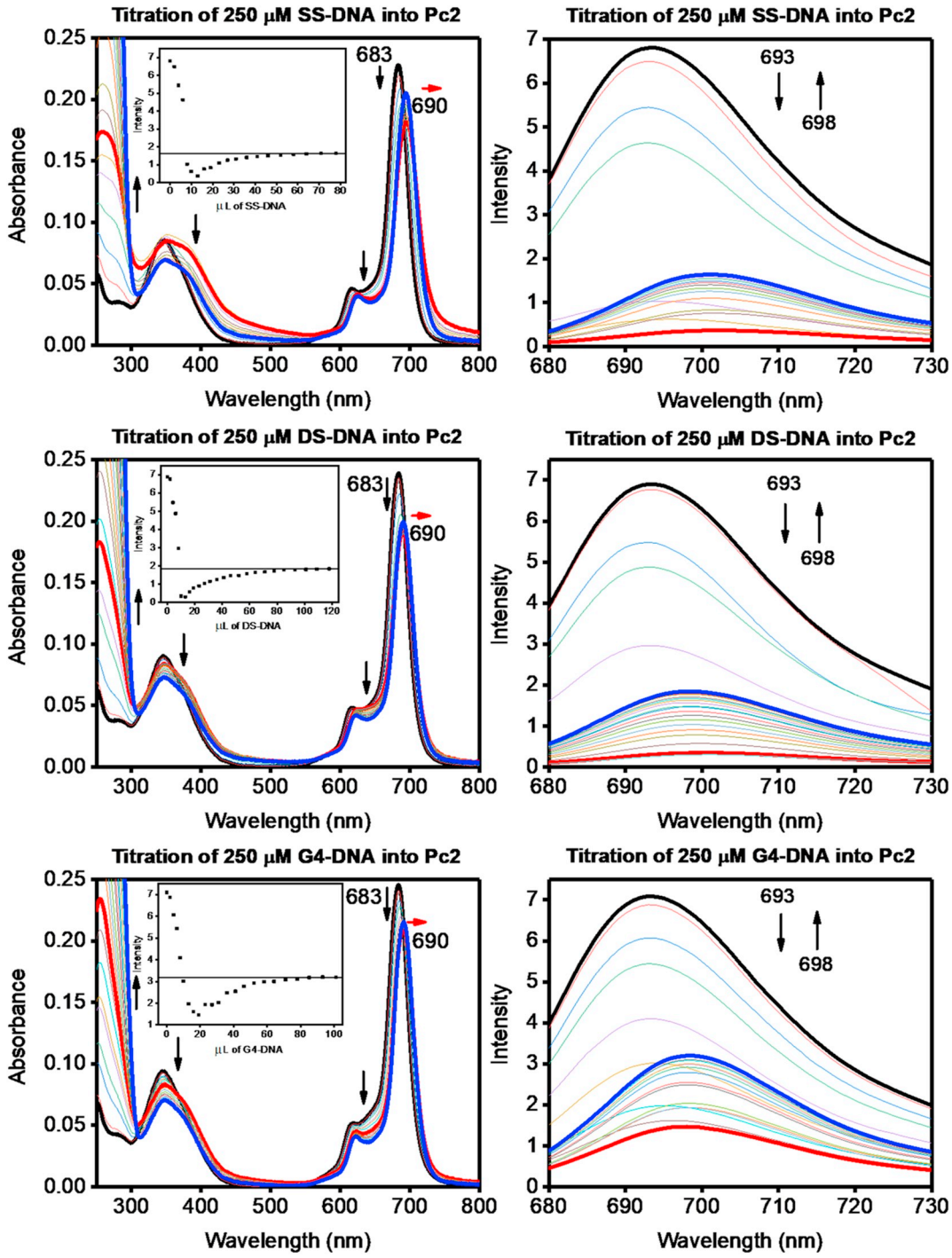

Fig. 8. UV–vis and fluorescence spectra of the DNA titrations involving **Pc2**.

or **Pc2** treated cells by live cell imaging. Remarkably, with only 1 min of irradiation, changes in cell morphology only 5 min into the experiment were observed for the **Pc2** treated cells (Fig. 10A).

Concurrent with the beginning of cell rounding, **Pc2** foci were observed and began to appear in the nucleus. Over the next 25 min, **Pc2** continued to accumulate in the nucleus, which proceeded to round and compact. At the final 30-minute time point, essentially all cells appeared apoptotic and **Pc2** formed the same compact foci that were observed in the compacted nuclei of the fixed cells (Fig. 9). **Pc1**-treated cells only showed marginal change in morphology after 15 min, albeit by the 30-minute time point, the **Pc1** treated cells are in the same state as the **Pc2** treated cells (Fig. 10b).

The change in localization from the cytoplasm to the nucleus by **Pc2** after irradiation offers potential insight into the mechanism of cell death. One possibility for the accumulation of **Pc2** in the nucleus after irradiation is membrane permeabilization by reactive oxygen species. This process involves dilating the endoplasmic reticulum, poking holes in the nuclear membrane, and allowing **Pc2** access to its preferred DNA binding partner. The morphological changes that occur simultaneously with **Pc2** re-localization are not mere symptoms of apoptosis but rather post-mortem events that occur, often hours after initiation of apoptosis [69]. However, we can detect morphological changes and re-localization of **Pc2** in as little as 5 min after irradiation. Mitochondrial outer membrane permeabilization occurs in late stage apoptosis and releases

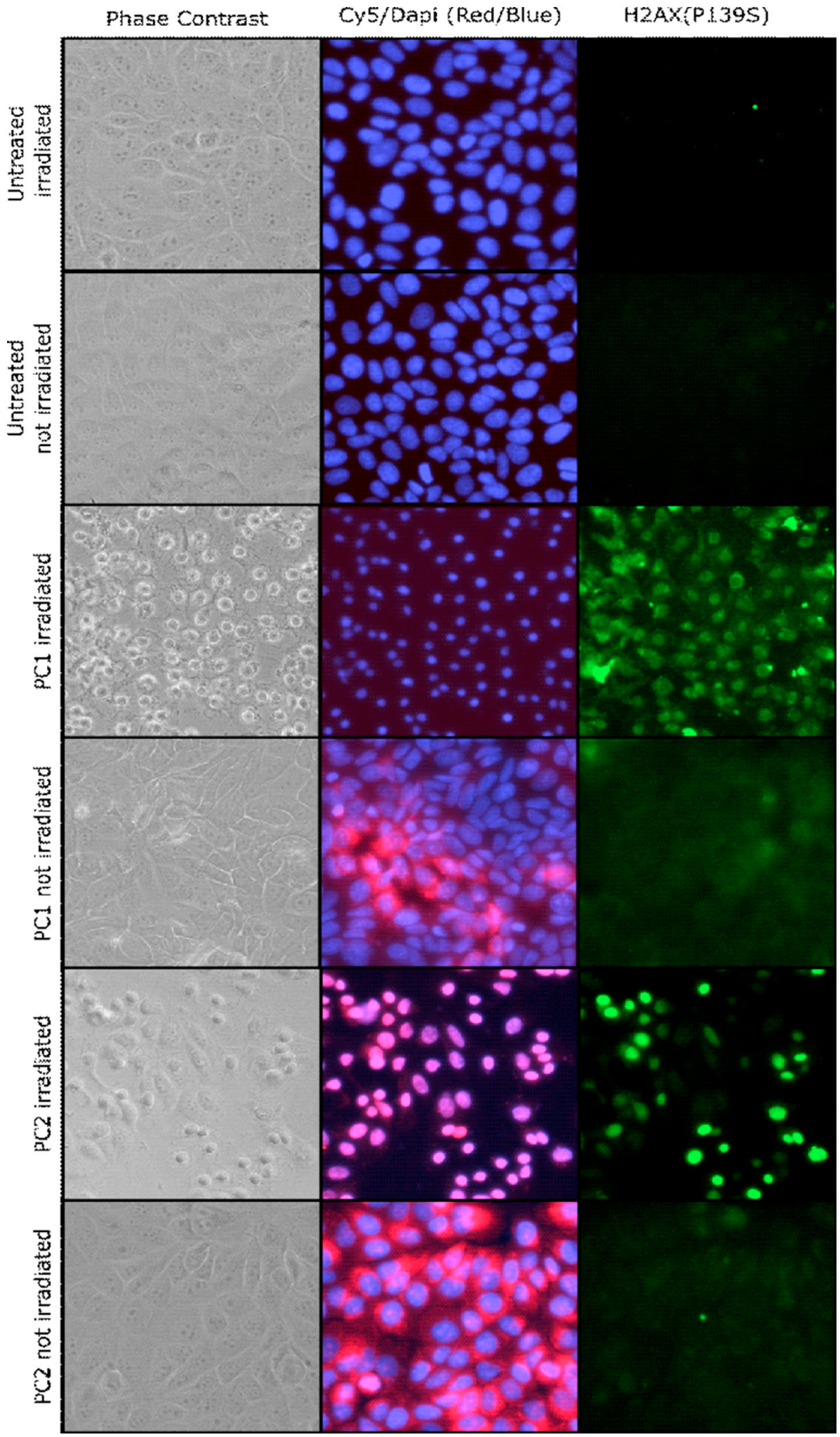

Fig. 9. Visualization of changes in cell morphology (phase contrast - grey), nuclear compaction (DAPI-blue) and DNA damage response (H2AX(P139S)-green) in MCF-7 cells in response to treatment with and excitation of **Pc1** and **Pc2** compounds. Where possible the CY5 channel (red) was used to monitor the phthalocyanine compound.

caspase enzymes into the cytoplasm, essentially committing the cell to death in as little as 10 min [70]. Membrane permeabilization by ROS generation was a mechanism proposed for a silicone phthalocyanine that is in clinical trial for treating cutaneous neoplasms [71,72]. Rapid ROS production by **Pc1** and **Pc2** during irradiation leading to membrane permeabilization is consistent with the observed cell death

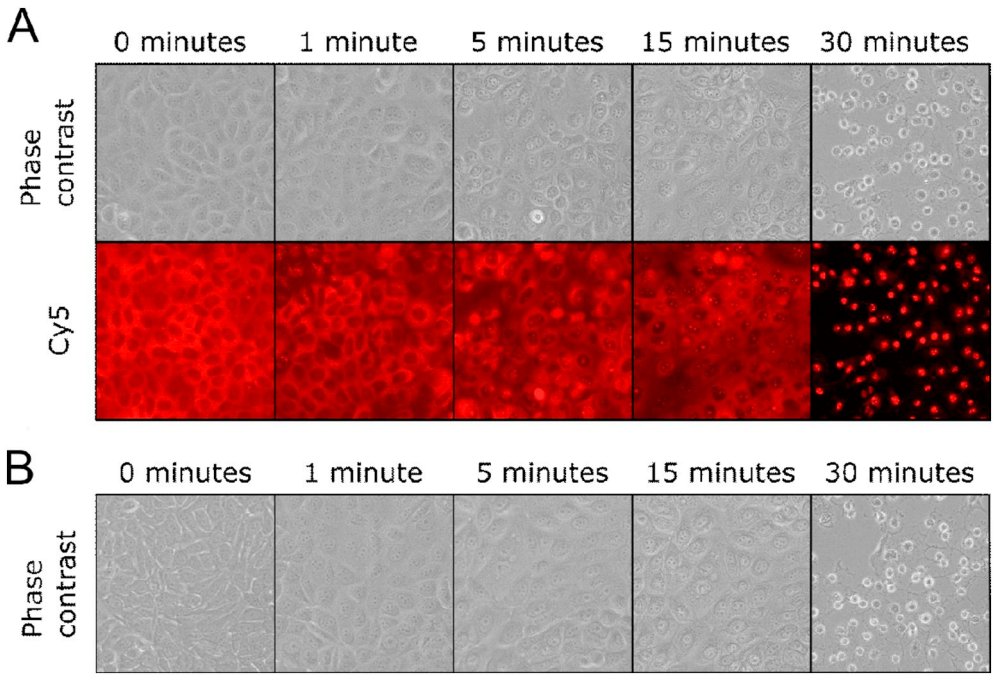

Fig. 10. Live cell imaging of MCF-7 cells treated with **Pc2** (A) or **Pc1** (B) and irradiated for 1 min, and monitored at time points for 30 min. The Cy5 channel allowed tracking of the **Pc2** dye throughout the course of the experiment.

timeline as well as the re-localization of **Pc2** after irradiation.

4. Conclusions

Two cationic zinc phthalocyanine photosensitizers (**Pc1** and **Pc2**) have been tested for DNA binding with three different DNA structures. It has been shown that tetracationic **Pc1** is highly aggregated while octacationic **Pc2** stays predominantly monomeric in aqueous solution, and both have high binding affinities to SS-DNA, DS-DNA and G4-DNA under physiological conditions. The photodynamic activity of the **Pc1** and **Pc2** photosensitizers was demonstrated with *in vitro* experiments, which indicated a strong potential for the use of these photosensitizers in the photodynamic therapy of cancer. It was found that the photodynamic action in the *in vitro* experiments differ significantly from each other as **Pc1** is less stable than **Pc2**. Both **Pc1** and **Pc2** are mostly present in the cytoplasmic area pre-irradiation; however, only the **Pc2** photosensitizer was observed to be localized in the cell nuclei post-irradiation, while the **Pc1** photosensitizer decayed upon visible light exposure. Both photosensitizers are very efficient in the generation of single oxygen species which results in high phototoxicity and apoptosis of cells.

Acknowledgements

This work was supported by the Minnesota Supercomputing Institute, NSERC, CFI, University of Manitoba, and WestGrid Canada. We also would like to acknowledge Professor Lukyanets for the samples of **Pc1** and **Pc2**.

References

[1] M. Casarin, S. Carlotto, Eur. J. Inorg. Chem. (2018) 3145–3155.
[2] S. Fu, C. Du, M. Zhang, A. Tian, X. Zhang, Prog. Org. Coat. 73 (2012) 149–154.
[3] D. Woehrle, G. Schnurpfeil, S.G. Makarov, A. Kazarin, O.N. Suvorova, Macroheterocycles 5 (2012) 191–202.
[4] G. Lincke, Dyes Pigments 59 (2003) 1–24.
[5] E.W.K. Schwartz, Text. Color. 62 (1940) 25–29.
[6] G. Peter, J. Porphyrins Phthalocyanines 4 (4) (2000) 432–437.
[7] Y. Xiao, L. Zhang, F. Peng, G.-B. Pan, RSC Adv. 8 (2018) 5344–5349.
[8] V.E. Pushkarev, L.G. Tomilova, V.N. Nemykin, Coord. Chem. Rev. 319 (2016) 110–179.
[9] M. Bouvet, P. Gaudillat, J.-M. Suisse, J. Porphyrins Phthalocyanines 17 (2013) 628–635.
[10] T. Choi, T.D. Milster, Opt. Eng. 45 (2006) 064302.
[11] H.S. Majumdar, A. Bandyopadhyay, A.J. Pal, Org. Electron. 4 (1) (2003) 39–44.
[12] A.A. Krasnovskii, G.P. Brin, Dokl. Akad. Nauk SSSR 53 (1946) 443–446.
[13] I.M. Geraskin, O. Pavlova, H.M. Neu, M.S. Yusubov, V.N. Nemykin, V.V. Zhdankin, Adv. Synth. Catal. 351 (2009) 733–737.
[14] A.B. Sorokin, Chem. Rev. 113 (2013) 8152–8191.
[15] B. Meunier, A. Sorokin, Acc. Chem. Res. 30 (1997) 470–476.
[16] P. Afanasiev, A.B. Sorokin, Acc. Chem. Res. 49 (2016) 583–593.
[17] E.A. Lukyanets, J. Porphyrins Phthalocyanines 3 (1999) 424–432.
[18] A. Fraix, S. Sortino, Photochem. Photobiol. Sci. 17 (2018) 1709–1727.
[19] P. Calzavara-Pinton, M.T. Rossi, R. Sala, M. Venturini, Photochem. Photobiol. 88 (2012) 512–522.
[20] L.B. Josefsen, R.W. Boyle, Theranostics 2 (2012) 916–966.
[21] A.E. O'Connor, W.M. Gallagher, A.T. Byrne, Photochem. Photobiol. 85 (2009) 1053–1074.
[22] R. Bonnett, Chem. Soc. Rev. 24 (1995) 19–33.
[23] E. Ben-Hur, I. Rosenthal, Photochem. Photobiol. 42 (2) (1985) 129–133.
[24] C. Milanesi, R. Biolo, E. Reddi, G. Jori, Photochem. Photobiol. 46 (5) (1987) 675–681.
[25] E.A. Lukyanets, V.N. Nemykin, J. Porphyrins Phthalocyanines 14 (2010) 1–40.
[26] N.C. López Zeballos, G.A. Gauna, M.C. García Vior, J. Awruch, L.E. Dicelio, J. Photochem. Photobiol. B 136 (2014) 29–33.
[27] L. Ozalp, S. Sağ Erdem, B. Yüce-Dursun, Ö. Mutlu, M. Özbil, Comput. Biol. Chem. 77 (2018) 87–96.
[28] J. Alzeer, N.W. Luedtke, Biochemistry 49 (2010) 4339–4348.
[29] D. Samaroo, M. Vinodu, X. Chen, C.M. Drain, J. Comb. Chem. 9 (2007) 998–1011.
[30] N.A. Kuznetsova, N.S. Gretsova, V.M. Derkacheva, O.L. Kaliya, E.A. Lukyanets, J. Porphyrins Phthalocyanines 7 (2003) 147–154.
[31] V.V. Sokolov, E.F. Stranadko, N.N. Zharkova, R.I. Iakubovskaia, E.V. Filonenko, T.A. Astrakhankina, Vopr. Onkol. 41 (2) (1995) 134–138.
[32] H. Lin, J. Chen, Y. Zhang, A. Ulla, J. Liu, F. Lin, L. Jiang, M. Huang, J. Inorg. Biochem. 189 (2018) 192–198.
[33] B. Ghazal, E.N. Kaya, A. Husain, A. Ganesan, M. Durmus, S. Makhseed, J. Porphyrins Phthalocyanines 23 (1/2) (2019) 46–55.
[34] D.A. Makarov, O.A. Yuzhakova, L.K. Slivka, N.A. Kuznetsova, V.M. Negrimovsky, O.L. Kaliya, E.A. Lukyanets, J. Porphyrins Phthalocyanines 11 (2007) 586–595.
[35] V. Cakir, D. Cakir, M. Piskin, M. Durmus, Z. Biyiklioglu, J. Organomet. Chem. 783 (2015) 120–129.
[36] D. Evren, A.K. Burat, I. Ozcesmeci, B.S. Sesalan, Dyes Pigments 96 (2013) 475–482.
[37] M.D. Maree, N. Kuznetsova, T. Nyokong, J. Photochem. Photobiol. A Chem. 140 (2001) 117–125.
[38] E.P. Booy, E.K.S. McRae, P. Ezzati, T. Choi, D. Gussakovsky, S.A. McKenna, Nucleic Acids Res. 46 (2018) 19–24.
[39] M.J. Frisch, G.W. Trucks, H.B. Schlegel, G.E. Scuseria, et al., Gaussian 09, Revision E.1, Gaussian, Inc., Wallingford CT, 2009 (For full citation, see Supporting Information).

[40] J.M. Tao, J.P. Perdew, V.N. Staroverov, G.E. Scuseria, Phys. Rev. Lett. 91 (2003) 146401.
[41] N. Godbout, D.R. Salahub, J. Andzelm, E. Wimmer, Can. J. Chem. 70 (1992) 560–571.
[42] Tenderholt, A. L. QMForge, Version 2.1. Stanford University, Stanford, CA, USA.
[43] Y. Jiang, C. Liu, X. Wang, T. Wang, J. Jiang, Langmuir 33 (2017) 7239–7247.
[44] I. M. Lipatova, E. A. Chernova, A. A.; Yusova, Makrogeterotsikly 10 (2017) 334–339.
[45] S. Doria, A. Lapini, M. Di Donato, R. Righini, N. Azzaroli, A. Iagatti, J.R. Caram, T.S. Sinclair, L. Cupellini, S. Jurinovich, B. Mennucci, G. Zanotti, A.M. Paoletti, G. Pennesi, P. Foggi, Phys. Chem. Chem. Phys. 20 (2018) 22331–22341.
[46] C. Jing, R. Wang, H. Ou, A. Li, Y. An, S. Guo, L. Shi, Chem. Commun. 54 (2018) 3985–3988.
[47] S. Kakade, R. Ghosh, D.K. Palit, J. Phys. Chem. C 116 (2012) 15155–15166.
[48] H. Isago, H. Fujita, J. Porphyrins Phthalocyanines 22 (2018) 102–111.
[49] V. Novakova, P. Reimerova, J. Svec, D. Suchan, M. Miletin, H.M. Rhoda, V.N. Nemykin, P. Zimcik, Dalton Trans. 44 (2015) 13220–13233.
[50] T.T. Tasso, T. Furuyama, N. Kobayashi, Inorg. Chem. 52 (2013) 9206–9215.
[51] T. Nyokong, H. Isago, J. Porphyrins Phthalocyanines 8 (2004) 1083–1090.
[52] N. Kobayashi, R. Higashi, K. Ishii, K. Hatsusaka, K. Ohta, Bull. Chem. Soc. Jpn. 72 (1999) 1263–1271.
[53] M. Gouterman, J. Mol. Spectrosc. 6 (1961) 138–163.
[54] M. Gouterman, G.H. Wagnière, L.C. Snyder, J. Mol. Spectrosc. 11 (1963) 108–127.
[55] R.V. Belosludov, D. Nevonen, H.M. Rhoda, J.R. Sabin, V.N. Nemykin, J. Phys. Chem. A 123 (2019) 132–152.
[56] N. Kobayashi, H. Ogata, N. Nonaka, E.A. Luk'yanets, Chem. Eur. J. 9 (2003) 5123–5134.
[57] T. Keles, B. Barut, A. Ozel, Z. Biyiklioglu, Dyes Pigments 164 (2019) 372–383.
[58] A. Arslantas, M.S. Agirtas, Turk. J. Chem. 42 (2018) 1310–1320.
[59] H. Bas, B. Barut, Z. Biyiklioglu, A. Ozel, Dyes Pigments 160 (2019) 136–144.
[60] C.C. Jayme, I.R. Calori, E.M.F. Cunha, A.C. Tedesco, Spectrochim. Acta A 201 (2018) 242–248.
[61] A. Arslantas, M.S. Agirtas, ChemistrySelect 3 (2018) 1755–1760.
[62] E. Bagda, E. Bagda, M. Durmus, J. Photochem. Photobiol. B Biol. 175 (2017) 9–19.
[63] B. Barut, A. Sofuoglu, Z. Biyiklioglu, A. Ozel, Dalton Trans. 45 (2016) 14301–14310.
[64] X.-F. Zhang, Q. Xi, J. Zhao, J. Mater. Chem. 20 (2010) 6726–6733.
[65] Z. Chen, C. Zhong, Z. Zhang, Z. Li, L. Niu, Y. Bin, F. Zhang, J. Phys. Chem. B 112 (2008) 7387–7394.
[66] G. Hacker, Cell Tissue Res. 301 (2000) 5–17.
[67] N.L. Oleinick, H.H. Evans, Radiat. Res. 150 (1998) 146–156.
[68] A.P. Castano, T.N. Demidova, M.R. Hamblin, Photodiagn. Photodyn. Ther. 2 (2005) 1–23.
[69] S. Elmore, Toxicol. Pathol. 35 (2007) 495–516.
[70] D.R. Green, Cell 121 (2005) 671–674.
[71] M. Lam, N.L. Oleinick, A.L. Nieminen, J. Biol. Chem. 276 (2001) 47379–47386.
[72] E.D. Baron, C.L. Malbasa, D. Santo-Domingo, F. P, J.D. Miller, K.K. Hanneman, A.H. Hsia, L. Nancy, V.C. Colussi, K.D. Cooper, Lasers Surg. Med. 42 (2010) 728–735.